Journal of King Saud University - Science 35 (2023) 102972

HOSTED BY

Contents lists available at ScienceDirect

Journal of King Saud University - Science

journal homepage: www.sciencedirect.com

Cytotoxicity of silver nanoparticles green-synthesized using *Olea europaea* fruit extract on MCF7 and T47D cancer cell lines

Njud S. Alharbi [a,*,1], Afnan I. Felimban [a,b,1]

[a] Department of Biological Sciences, Faculty of Science, King Abdulaziz University, Jeddah 21589, Saudi Arabia
[b] Regenerative Medicine Unit, King Fahad Medical Research Center, King Abdulaziz University, Jeddah, Saudi Arabia

ARTICLE INFO

Keywords:
Green synthesis
Silver nanoparticles
Olea europaea
Breast cancer cells
Cytotoxic activity
Therapeutic agents

ABSTRACT

To develop a more environmentally friendly, low-cost, energy-efficient, and non-toxic strategy for producing silver nanoparticles (AgNPs) for cancer therapy, in this study, we established a green synthesis method using *Olea europaea* fruit extract (OFE) as a reducing and stabilizing agent for the AgNPs. The AgNPs were then characterized using relevant spectroscopy and other analyses, and their cytotoxicity on two breast cancer cells, MCF7 and T47D, were evaluated. The AgNPs exhibited considerable anticancer potential against both MCF7 and T47D cells, inhibiting their proliferation more efficiently than the OFE. The AgNPs-OFE was highly cytotoxic against the T47D cancer cell line with a 50 % inhibitory concentration (IC_{50}) of 77 μg/mL. This study demonstrates the feasibility of using OFE in green synthesizing stable AgNPs with an acceptable particle size and shape and other desirable characteristics, including anticancer activities against the selected *in vitro* breast cancer cell model. The findings demonstrate the encouraging biomedical and therapeutic application of the Plant-derived AgNPs, which has clinical and academic relevance and warrants further investigation.

1. Introduction

Silver nanoparticles (AgNPs) have gained much attention because of their unique properties. Biological synthesis has been the focus of research studies as a low-cost, eco-friendly, energy-efficient, and non-toxic protocol for synthesizing AgNPs (Li et al., 2012; Saravanan et al., 2017; Hashemi et al., 2020). Biological synthesis is a vital tool for reducing Ag ions into AgNPs and is an alternative to chemical and physical techniques. Biological methods do not require high pressure and energy; hence, no additional toxic and hazardous chemicals are required, which could contribute to minimizing the risks of applying AgNPs to mammals (Salem and Fouda, 2021). Furthermore, surface coating AgNPs with non-toxic biomolecules in biological synthesis could make them even safer and more biocompatible (Amooaghaie et al., 2015). Plants in AgNPs synthesis are more beneficial than other biological methods due to the simplicity of growing plants (Asimuddin et al., 2020; Ma et al., 2021; Rajivgandhi et al., 2022). Additionaly, phytochemicals (e.g., polyphenols, flavonoids, tannins, and proteins) found in plants play a key role in reducing metal ions into NPs and coating NPs during green synthesis, which supports their stability and enhances their biomedical applications (Afreen et al., 2020).

Cancer is a genetic disease caused by the mutation, amplification, or abnormal expression of essential genes involved in cell fate regulation (Herceg and Hainaut, 2007). Although conventional cancer treatments are effective, they are expensive and can affect healthy tissues and organs. Thus, it is necessary to develop alternative, safe, and affordable techniques to inhibit cancer cell growth without damaging healthy cells. AgNPs are a good alternative that enables effective cancer treatment owing to their novel properties, including antiproliferative and apoptosis-inducing properties. AgNPs exert cytotoxicity by inducing reactive oxygen species (ROS), as previously reported (Foldbjerg et al., 2009). ROS levels are linked to the induction of apoptosis and necrotic cell death of some cell lines. Rajendran et al. (2022) showed that AgNPs synthesized using *Salvia leucantha* extract were effectively cytotoxic to the human lung cancer A549 cells. Bhat et al. (2022) examined the *in vitro* cytotoxicity of AgNPs biosynthesized using *Artocarpus lakoocha* fruit extract.

Furthermore, AgNPs have physical and reactivity properties and are helpful for research in various fields, including drug delivery (Khatik, 2022). Besides their high bioavailability, AgNPs are sustained and

Peer review under responsibility of King Saud University.
* Corresponding author.
E-mail addresses: nsfalharbi@kau.edu.sa (N.S. Alharbi), aifelimban@stu.kau.edu.sa (A.I. Felimban).
[1] Equal contributors: Njud S. Alharbi and Afnan I. Felimban contributed equally to this manuscript.

https://doi.org/10.1016/j.jksus.2023.102972
Received 11 June 2022; Received in revised form 8 June 2023; Accepted 25 October 2023
Available online 26 October 2023

controlled and can circulate for extended periods, with a higher capacity to load drugs. AgNPs penetrate cells more readily and can be directed at specific organs. AgNPs offer protection against enzymes, physiological pH, and moisture and can enter the body nasally, orally, parenterally, or intraocularly. Plant-derived AgNPs have been used in drug delivery and to cure cancer-related diseases (Lee et al., 2019).

Motivated by the above discussion, this study biosynthesized the AgNPs using *O. europaea* fruit extract (OFE), which is widely used as a therapeutic medicine because of its antioxidant properties associated with its high content of phenolic compounds (McDonald et al., 2001). Breast cancer has become the most diagnosed cancer, attracting research attention (Sung et al., 2021). Hence, this study also evaluated the anticancer activities of the AgNPs against MCF7 and T47D cells. The contributions of this work are follows. First, the study established a biosynthesis approach using OFE and optimized the synthesis conditions to produce AgNPs with high yield and precise morphologies. Second, the study evaluated the biosynthesized AgNPs' cytotoxicity against *in vitro* MCF7 and T47D cells. Furthermore, the AgNP-OFE's anticancer properties were examined using appropriate techniques and analyses. The results suggest that AgNPs-OFE could be potentially valuable cancer treatments, which would warrant further studies of their action mechanisms.

2. Materials and methods

2.1. Preparation of OFE

OFE was prepared as described previously (Kredy, 2018). The collected fruits were washed individually with running tap water, followed by distilled water, cut into pieces, left to dry, protected from direct light at 24 °C, and made into fine powders and stored in airtight containers. OFE was made by boiling 5 g of its fine powder with 100 mL of deionized water for 10 min. The extracts were cooled down and filtered through a coffee filter, followed by Whatman No. 1 filter paper. The prepared OFE was stocked in an appropriate bottle at –4 °C until use.

2.2. Optimization of the AgNPs synthesis

The AgNPs plants-mediated synthesis, as shown in Fig. 1, is a simple two-step process. The first step involves reducing silver ions (Ag +) to Ag, and the second is stabilization and agglomeration, leading to AgNPs forming. The hydroxyl groups involved in the plant's phytochemicals are mainly responsible for stabilizing and reducing Ag + to Ag° (Some et al., 2019). A further reduction of Ag^0 results in the growth of silver nuclei, which leads to the formation of AgNPs. Adjusting the synthesis parameters, including extract concentration, pH, temperature, and light intensity, helps control the AgNPs' morphology and yield. Also, the $AgNO_3$ concentration and the reaction time impact the morphology of AgNPs. The level of toxicity of plant-derived AgNPs may vary depending on the target cells, the extracted solvents, the collection site, and the study period.

This study biosynthesized the AgNPs using OFE and optimized the synthesis parameters (extract concentration, pH, temperature, and light intensity) to improve the AgNPs' quality. AgNPs were biosynthesized using a previously described method (Kredy, 2018). Three extract concentrations: 1, 2, and 3 mL, were separately added to 9 mL of 1 mM AgNO3 solution, resulting in mixture ratios of 1:9, 2:9, and 3:9. The AgNPs were biosynthesized at 40, 60, and 80 °C reaction temperatures. The AgNPs synthesis was investigated at three pH values: 4, 7, and 9, adjusted using 0.5 N acetic acid or 0.1 N sodium hydroxide. The reaction mixtures were kept under three conditions: sunlight, room light, and dark, to investigate the impact of light intensity on the AgNPs.

The solvent used in green synthesis is critical to the technique's success, and this study used the universal solvent, water, to avoid the potential toxicity of chemical substances and ensure safety regarding human health and the environment. The reduction of Ag + into Ag° was detected by the color change from yellowish to dark brownish. Notably, AgNPs exhibit a dark brown color in an aqueous solution due to the excitation of the surface plasmon vibrations in the metal nanoparticles (Saware & Venkataraman, 2014). A stable dark brown color proved that all Ag + ions have entirely reduced into AgNPs, as earlier reported (Rawat et al., 2020). Repeating centrifugation at 10,000 rpm for 10 min at 24 °C and washing with deionized water helped purify and obtain excess extracts. Purified AgNPs were collected and dried for further characterization and other analysis.

2.3. Characterization of AgNPs

Spectroscopic analysis of the biosynthesized AgNPs was performed using a Cary® 50 ultraviolet–visible (UV–Vis) spectrophotometer at wavelengths of 300–600 nm. A Fourier-transform infrared (FTIR) spectrometer was used at wavenumbers from 600 to 4000 cm^{-1} to analyze and identify the OFE biomolecules involved in forming and stabilizing the AgNP. Zeta potential measurements and dynamic light scattering (DLS) were used to evaluate the physical stability of the AgNP samples. They were also utilized to determine particle size using a zeta sizer Nano. In addition, field emission scanning electron microscopy (FESEM) was used to characterize the AgNPs' morphology, shape, and size.

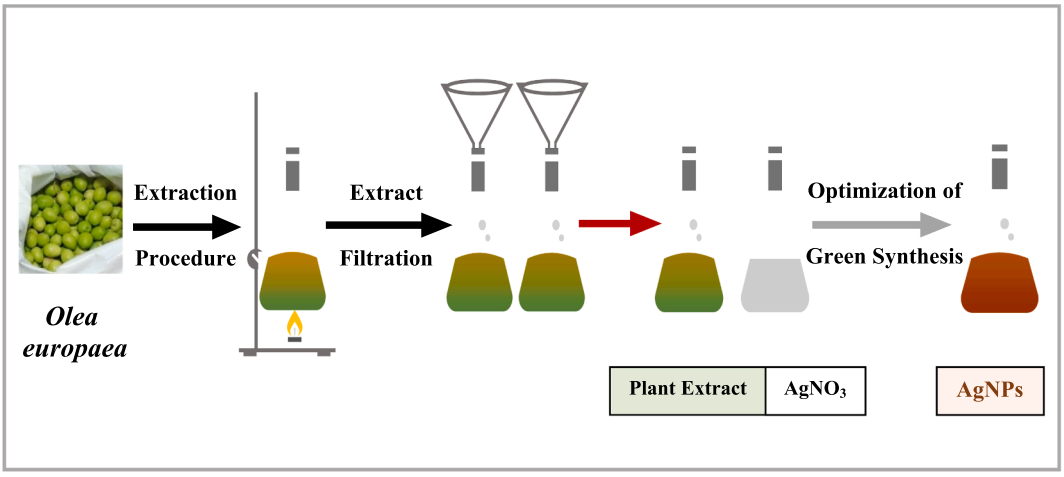

Fig. 1. Plant mediated synthesis of AgNPs.

2.4. Anticancer properties

2.4.1. Cell lines and cell cultures

MCF7 and T47D cancer cells were maintained in Dulbecco's Modified Eagle Medium (DMEM containing 10 % fetal bovine serum (FBS) and 1 % penicillin–streptomycin. The cell cultures were maintained at 37 °C in a 5 % CO2 humidified incubator and passaged at 80–90 % confluence. The morphology and the number of cells were checked regularly using an inverted microscope. Once the cell culture reached 80 % confluence, they trypsinized for subculturing with 0.25 % trypsin. They aspirated into a 15 mL centrifuge tube, setting up the cell culture hood for subculturing. Subculturing or passaging the cells was done by transferring some of the precipitate cells of the previous culture into a new growth medium.

2.4.2. Stock serial dilutions preparation

1 mg of dried AgNPs samples (biosynthesized using OFE) was dissolved in 1 mL of 3 % dimethyl sulfoxide (DMSO) to obtain 1 mg/mL of stock solution, referring to AgNPs, and in 1 mL of OFE to get 1 mg/mL of AgNPs-OFE. DMSO is commonly used to solubilize poorly soluble drugs and is considered safe at low concentrations of up to 10 %, as previously reported (Kloverpris et al., 2010). This study used 3 % of DMSO. All samples were then diluted to the required treatment concentrations: 25, 50, 100, 150, and 200 μg/mL for further examinations.

2.4.3. Cytotoxicity assay

We comparatively analyzed the cytotoxicity of all prepared samples (AgNPs, AgNPs-OFE, and OFE) against cancer cells using the MTT assay. Briefly, we seeded 5×10^3 cells per well in 90 μL medium/well in 96-well plates, which were then incubated overnight to allow them to reach confluence. The cells were treated in triplicate at different concentrations (25, 50, 100, 150, and 200 μg/mL), while the control cell culture wells were left untreated. We then incubated the plates for 24 h, discarded the medium, added 100 μL MTT solution to each well, and incubated them for approximately 3 h. Subsequently, we replaced the medium with 100 μL pure DMSO and measured the optical density of the resulting solution using a microplate reader at 570 nm. The the % cell viability was computed as:

$$\%\,\text{cell viability} = \frac{\text{Absorbance treated cells} - \text{Absorbance blank}}{\text{Absorbance control cells} - \text{Absorbance blank}} \times 100.$$

Blank refers to the background that means the medium, MTT solution, and DMSO.

2.4.4. Morphological changes

According to an earlier described approach (Mittal et al., 2020), morphological changes in the treated T47D cells were examined to confirm apoptotic features. The T47D cells were seeded at a density of 2 × 105 cells/well in a 6-well plate and incubated for 24 h. The cells were treated with the AgNPs-OFE at 200 μg/mL for 24 h, and morphological changes were observed under bright field inverted microscopy at 20 × magnification. The AgNPs-OFE at 200 μg/mL was used here as it had significant toxicity on the cancer cells (T47D) compared to other treatments (see Results Section).

2.4.5. Cell cycle analysis

The T47D cells were seeded and treated as earlier described and processed for cell cycle analysis. The cells were washed twice with 2 mL of phosphate-buffered saline (PBS) and centrifuged at 1500 rpm for 5 min. The cells were then fixed in chilled 70 % ethanol, maintained at –20 °C overnight, and centrifuged at 2000 rpm for 5 min after being rinsed twice with 3 mL PBS. The cells were mixed with 100 μL RNase and incubated at 37 °C. Then, 400 L of propidium iodide (PI) was used in the dark to stain the cells, which were examined using a FACSAria III flow cytometer.

2.4.6. Nuclear morphology analysis (DAPI staining)

As reported earlier (Mittal et al., 2020), the nuclei of the treated cells were stained with 4′,6-diamidino-2-phenylindole (DAPI) fluorescent dye. The cells were rinsed with PBS, fixed with 4 % paraformaldehyde (PFA), rinsed thrice with PBS, and stained with 100 μL DAPI in the dark for 10 min. The cells were then rinsed with PBS and observed under a fluorescence microscope.

2.4.7. DNA fragmentation

The treated cells were rinsed with PBS and centrifuged at 2000 rpm for 5 min to evaluate apoptosis. DNA was isolated using a QIAamp DNA mini kit. In a microcentrifuge tube, 20 μL proteinase K and 4 μL RNase A were added to 200 μL of the sample. Then, 200 μL Buffer AL was added and incubated for 10 min at 56 °C, followed by brief centrifugation at 8,000 rpm for 1 min. The supernatant was transferred to a sterile microcentrifuge tube. Then, 200 μL ethanol was added, followed by vortexing and brief centrifugation at 8,000 rpm for 1 min. Further, the column was placed in a clean 2 mL collection tube, and 500 μL of buffer AW1 was added and centrifuged at 8,000 rpm for 1 min. The column was transferred to another clean 2 mL collection tube with 500 μL of buffer AW2, followed by centrifugation at 8,000 rpm for 1 min. Next, the DNA was eluted with 100 μL elution buffer and stored at −20 until used. Finally, the DNA fragments were resolved by 1 % agarose gel electrophoresis visualized under a UV transilluminator and photographed.

2.4.8. Statistical analyses

The study conducted the experiments in triplicate and analyzed the results using SPSS software. The statistical significance was computed using a one-way analysis of variance (ANOVA) and Tukey's post hoc tests.

3. Results and discussion

3.1. Optimization of the AgNPs synthesis

This study tested the production of AgNPs with different parameters to optimize the AgNPs for antitumor applications. Fig. 2a shows that the absorbance of AgNPs increases when the extract concentration increases. The highest absorbance was achieved in the ratio of 3:9. A more intense color was formed when the extract concentration was increased since more biomolecules were present. At higher extract concentrations, biomolecules serve as reducing agents and as coating and stabilizing agents, preventing the aggregation of the nanoparticles, and influencing their size. The results also show that higher temperatures produced higher rates of AgNPs formation with decreased wavelength (Fig. 2b), indicating the formation of small-sized AgNPs. Increasing temperature will increase the molecule's kinetic energy, rapidly reducing silver ions. When silver ions are consumed very fast, it leaves fewer opportunities for the synthesized nanoparticles to grow.

Moreover, the alkaline condition (pH = 9) displayed the highest reaction rate due to the increased availability of functional groups, efficiently synthesizing small AgNPs (Fig. 2c). The pH can alter the biomolecules' electric charges, influencing the coating and stabilizing processes and, consequently, the growth of AgNPs. The results also reveal that the nanoparticles' size decreased with increasing pH, indicating lower aggregation and more effective stabilization. In contrast, due to the positively charged functional groups, the bio-reduction was mainly accomplished at a pH value of 4 by ionic bonding and biomolecules. Consequently, numerous biomolecules bind during the biosynthesis of AgNPs, causing agglomeration and forming larger particles. Therefore, adjusting the pH can help control the AgNPs' size and stability, improving their properties and expanding their applications. The findings also confirm that sunlight can accelerate AgNPs synthesis, producing stable AgNPs with high yields (Fig. 2d). Photons from sunlight could accelerate the synthesis reaction, rapidly producing AgNPs (Raut et al., 2014; Nguyen, 2020). Synthesis parameters with the best

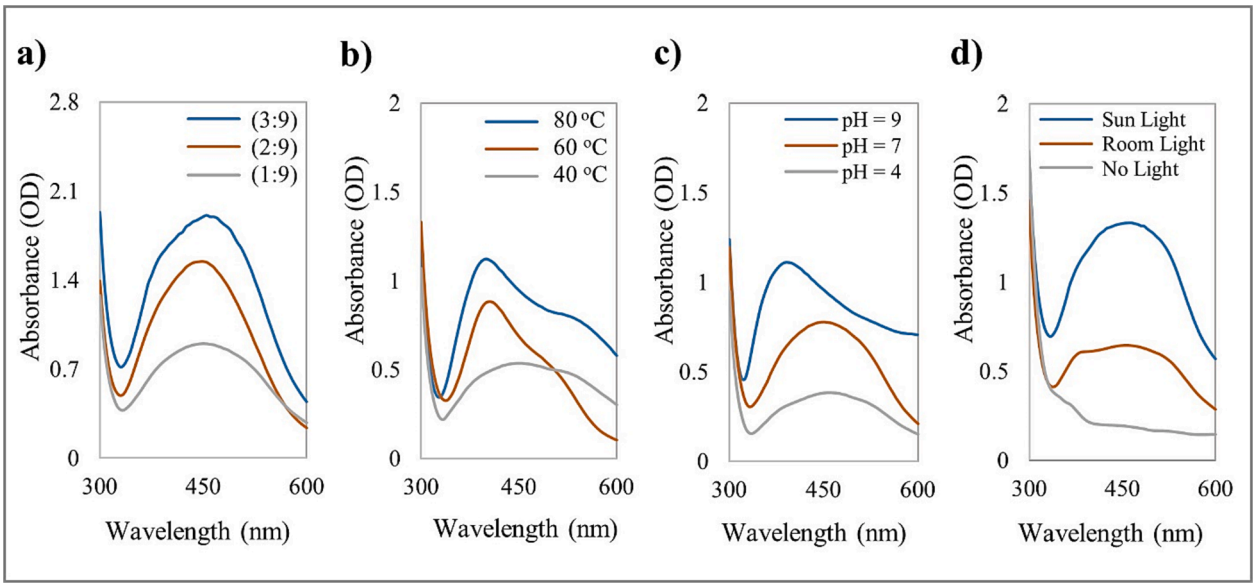

Fig. 2. UV–Vis spectrum of AgNPs biosynthesized from *O. europaea* fruit extract at (a) different extract concentrations, (b) different temperatures, (c) different pH values, and (d) different light intensity conditions.

achievements were selected to set the optimum operating conditions (3:9 plant extract to $AgNO_3$, 80 °C, pH value of 9, and sunlight) for further synthesis and characterization.

3.2. Characterization of AgNPs

UV–Vis spectral analysis revealed a strong absorbance peak at 440 nm (Fig. 3), indicating the SPR of AgNPs. In Fig. 4, FTIR analysis results showed a broad peak at 3309.38 cm^{-1}, indicating a hydroxyl functional group, thus confirming the presence of flavonoids and polyphenols. The bio-compounds in the OFE were adsorbed on the AgNPs' surface. DLS analysis showed that the AgNPs had an average hydrodynamic size and polydispersity index (PDI) of 67.51 nm and 0.24, respectively, which is generally accepted. Smaller PDI indicates more homogeneity in the NP produced. The zeta potential of − 23 mV with a signal peak (Fig. 5) indicated that AgNPs had a moderate stability that was prolonged in solution. The zeta potential of the AgNPs provided a general idea about their surface charge and stability based on the measured electrophoretic mobility of the samples in an electric field (Shukla et al., 2008).

The FESEM analysis showed that the biosynthesized AgNPs were almost spherical and ranging in size from 20.5 to 33.2 nm, with some aggregation (Fig. 6). The AgNPs aggregation observed could be attributed to the high concentration and solvent removal during the sample preparation, resulting in electrostatic forces, causing the particles to aggregate. This aggregation could lead to variations in the size of the biosynthesized AgNPs. Robustly coating the AgNPs can enhance their stability, protecting against agglomeration and aggregation (Selvan et al., 2018). DLS analysis results showed a larger particle size (67.51 nm) than that obtained with FESEM analysis (33.2 nm), as expected as FESEM measures the hydrodynamic size of the AgNPs, including hydration layer, polymer shells, or other possible stabilizers, as explained earlier (Mohanta et al., 2016).

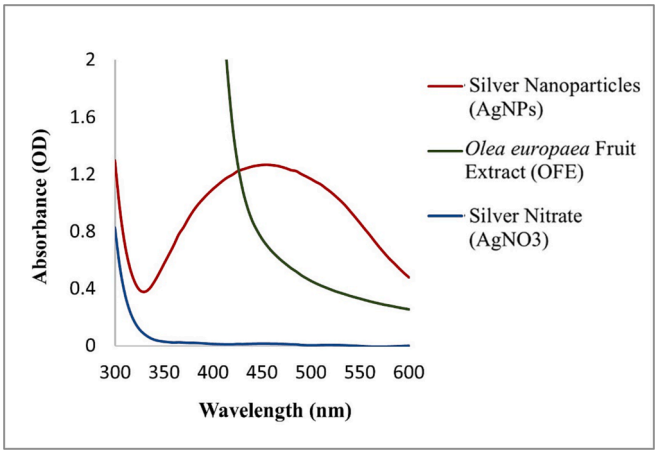

Fig. 3. UV–Vis spectra of AgNPs biosynthesized under the optimum conditions (3:9 plant extract to AgNO3, 80 °C, pH value of 9, and sunlight).

3.3. Anticancer properties

Fig. 7 shows the recorded growth rates of the cancer cells (MCF7 and T47D) after 24 h exposure to various concentrations of AgNPs, OFE, and AgNPs-OFE. The cell viability decreased in a concentration-dependent manner of sample exposure. Treatment of T47D cells with 200 µg/mL AgNPs, OFE, and AgNPs-OFE samples for 24 h significantly decreased the cell viability from 100 % (untreated cells) to 33, 39, and 29 %, respectively. The respective IC_{50} values of the samples were 94, 143, and 77 µg/mL. These findings confirm the significant reduction in cell viability from 100 % (untreated cells) to 33 % is attributed to the biosynthesized AgNPs, and a further decrease to 29 % could be achieved if the AgNPs dissolved in OFE instead of DMSO. T47D cells were more sensitive to AgNP-OFE than AgNPs or OFE. In contrast, MCF7 cells exhibited less sensitivity to OFE and AgNPs-OFE than AgNPs. Also, the OFE considerably decreased the cell viability from 100 % (untreated cells) to 39, and 44 % in the treated T47D and MCF7 cells, respectively. Therefore, this study further investigated treating the T47D cells with AgNP-OFE to evaluate their anticancer properties. The potential anticancer efficiency of the AgNPs-OFE could be attributed to the superficial coating of phytoconstituents and their smaller size. Que et al. (2019) demonstrated that smaller nanoparticles have stronger anticancer activity owing to their large specific surface area, thus, having more active sites. A possible explanation is that small-sized nanoparticles can enter cells via endocytosis or direct diffusion.

In Fig. 8, the cytometric measurement of PI-stained control showed a significant cell population in the G0/G1 phase, indicating cell proliferation. In contrast, in treated cells, the results show a decrease in the cell population in the G0/G1 phase concomitant with a remarkable increase

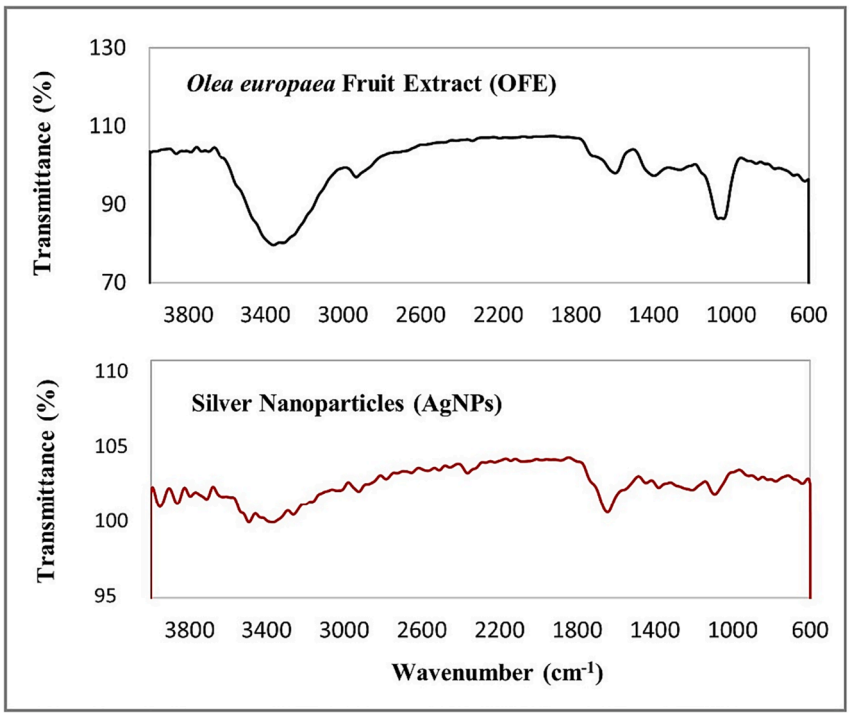

Fig. 4. FTIR spectra of biosynthesized AgNPs and OFE.

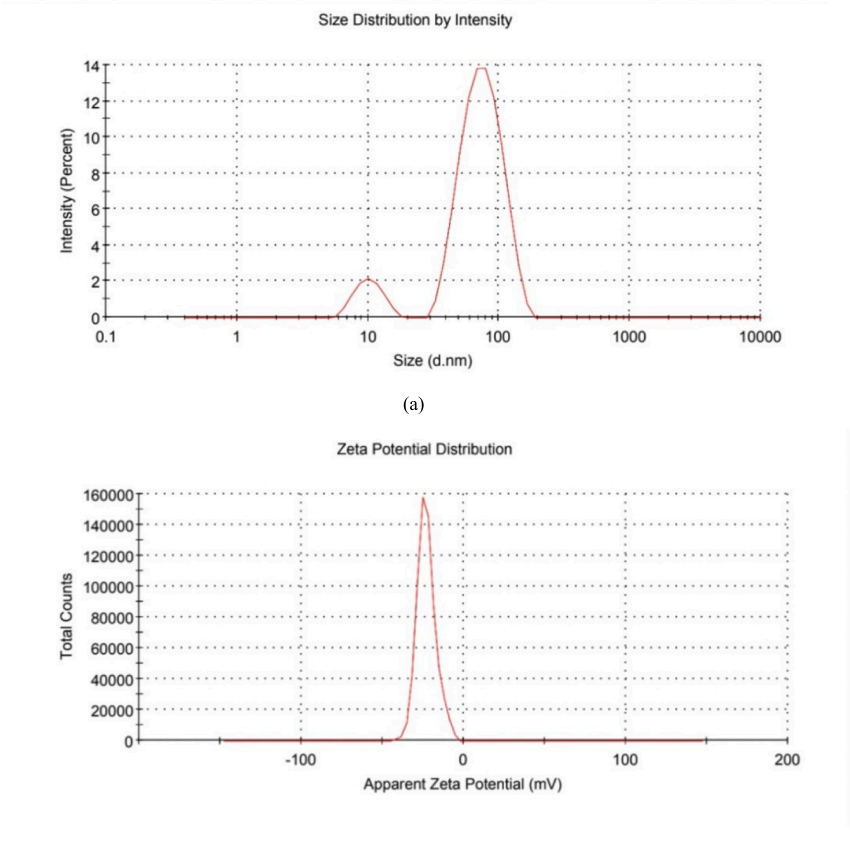

Fig. 5. (a) Particle size distribution and (b) zeta potential of biosynthesized AgNPs.

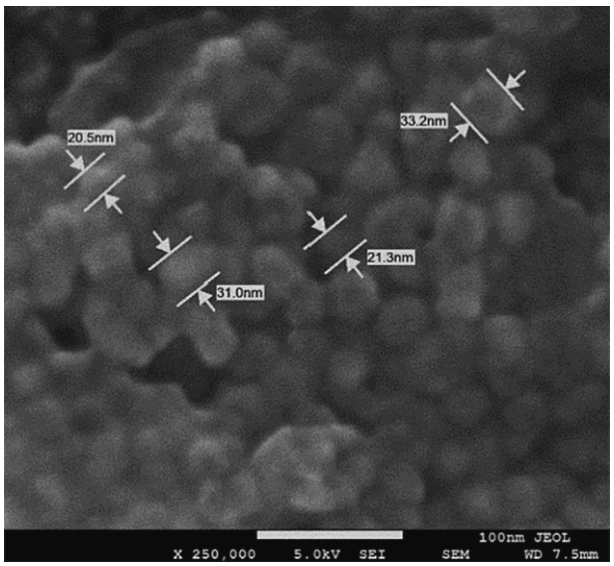

Fig. 6. FESEM image of biosynthesized AgNPs.

in the SubG1 phase. Accumulation of cells in the SubG1 phase strongly suggests DNA damage and cells undergoing apoptosis/necrosis. The decrease in the G0/G1 population indicates that a limited number of cells entered the cell cycle. The increase in the SubG1 (apoptotic) population means that treated cells could not pass through the next checkpoint; thus, AgNPs-OFE induced cell cycle arrest in the treated cells. The DAPI staining and DNA fragmentation assay results supported the present flow cytometry results.

Fig. 9a show that the untreated cells (control) maintained their original morphology, as polygonal or trigonal in shape, with intact cell membranes. In contrast, the treated cells lost their original morphology and became spherical, with evident cell shrinkage (Fig. 9b). The number of treated cells decreased as the dead cells detached from the surface, suggesting that AgNP-OFE caused significant cellular morphology, growth, and attachment changes in the treated cells. Furthermore, Untreated cells displayed normal nuclei, whereas treated cells showed apoptotic nuclei (Fig. 9c and 9d). A nuclear morphology analysis revealed some characteristic features of apoptosis, including nuclei cracking, chromatin condensation, and fragmentation. Besides, the treated cells showed reduced blue fluorescence intensity compared to the untreated cells, indicating apoptosis. In addition, fragmentation of genomic DNA is an essential feature for the detection of apoptosis. An Agarose Gel DNA fragmentation assay was performed to investigate the induction of apoptosis and DNA damage caused by AgNP-OFE. Fragmented DNA ladders were observed in treated cells (Fig. 10), indicating the induction of apoptosis following exposure to AgNP-OFE. In contrast, untreated cells (control) showed no fragmented DNA in the lane.

The ability of a treatment to selectively cause apoptosis in cancer cells while sparing healthy cells is an essential requirement for effective cancer treatment (Jang et al., 2016). In this regard, earlier investigations reported that AgNPs were less toxic to healthy cells than cancer cells (Grande et al., 2020), highlighting the potential application of AgNPs as an anticancer treatment. For instance, Singh et al. (2021) demonstrated a deficient level of toxicity of the AgNPs produced from *papaya* leaf extract against normal HaCaT cells, and Farahani et al. (2022) also reported less toxicity of the AgNPs biosynthesized using *Amigdalus spinosissima* against normal L929 cells.

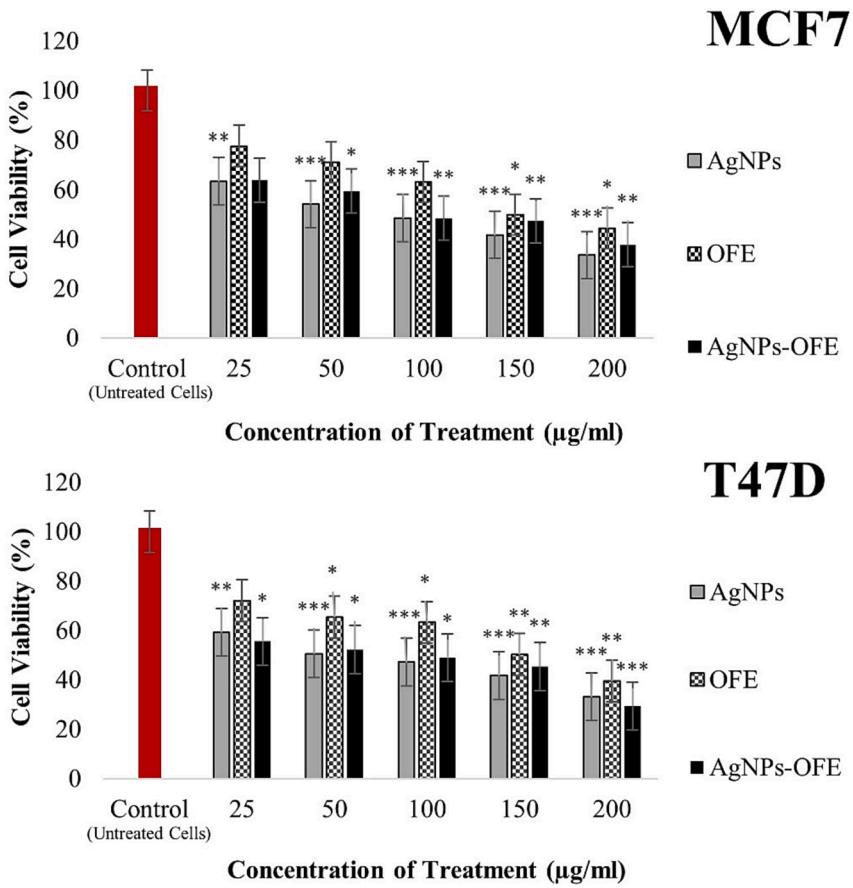

Fig. 7. Cytotoxicity of AgNPs, OFE, and both (AgNP-OFE) on viability of MCF7 and T47D cancer cells after 24 h exposure. * $P < 0.05$, ** $P < 0.01$, and ***$P < 0.001$ compared with untreated cells.

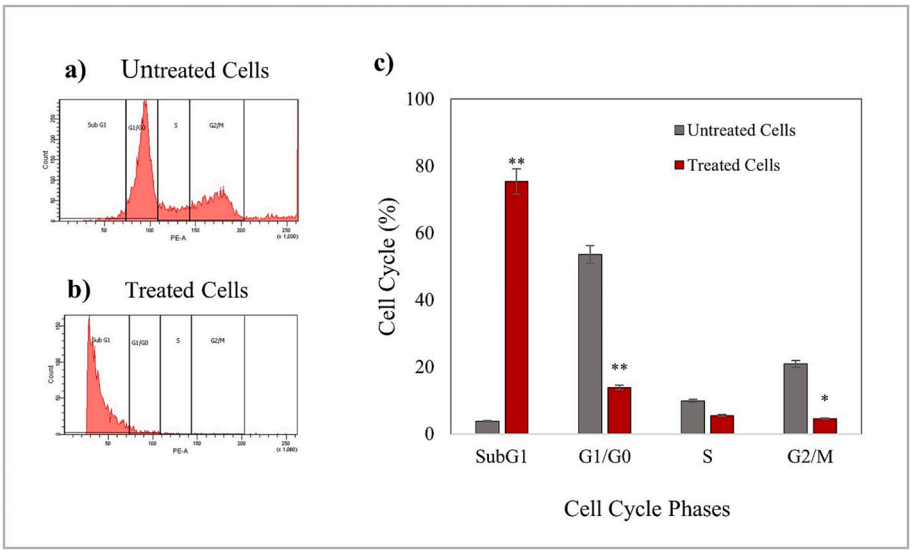

Fig. 8. Cell cycle analysis in T47D cells exposed to 200 μg/mL AgNP-OFE for 24 h. Results are represented as mean ± standard deviation. Data are statistically significant with $*p < 0.05$, when compared with control.

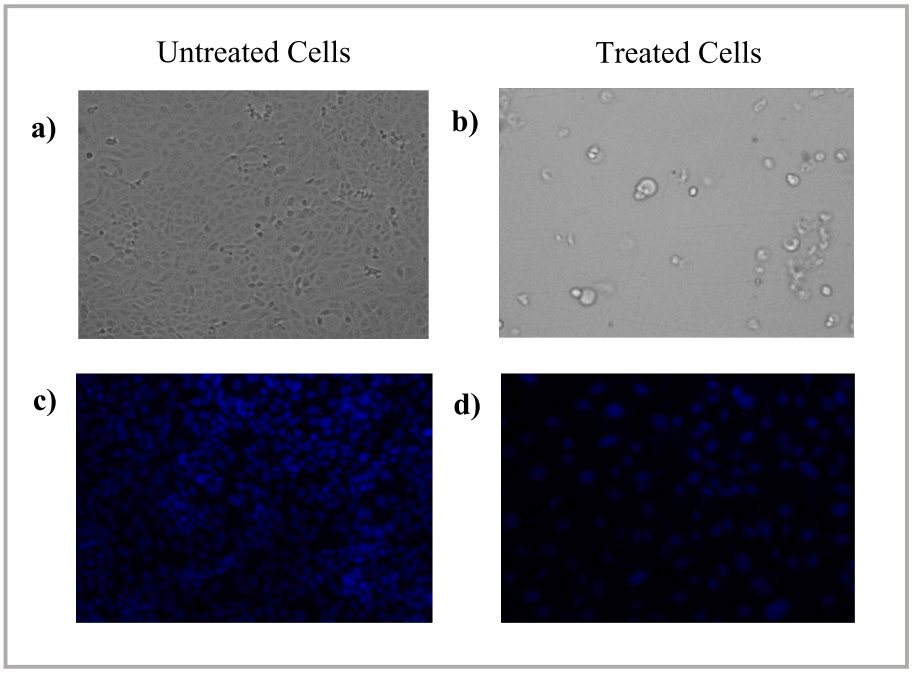

Fig. 9. Morphological changes in T47D cells exposed to 200 μg/mL AgNP-OFE for 24 h detected using bright field microscopy and fluorescence microscopy. (a) morphological changes in untreated cells (control), (b) morphological changes in treated cells, (c) DAPI staining of untreated cells, and (d) DAPI staining of treated cells.

Although a few studies used *O. europaea* extracts to synthesize AgNPs, none applied sunlight to accelerate the AgNPs synthesis. The current study biosynthesized the AgNPs using OFE and sunlight, achieving a quick bio-reduction and high dispersion of small stable AgNPs with high yield. Further investigations of green synthesis would help maintain the characteristics of the nanoparticles to produce high-quality AgNPs, offering promising potential in many biomedical applications, such as treating deadly diseases and fighting undesirable pathogens. The findings show the good biomedical and therapeutic applicability of the plant-mediated AgNPs, which is clinically and academically relevant and warrants further investigation. The limitation of this research also points toward essential issues that need to be investigated in the future. Determining the fundamental role of the plant's phytochemical components in the reduction reactions and coating processes that control the nanoparticles' size, shape, and stability is challenging. Also, factors such as agglomeration and aggregation may affect the AgNPs' efficiency and should be extensively investigated. Furthermore, this study is based on *in vitro* experiments, and evaluating the nanoparticles' biosafety and biocompatibility *in vivo* experiments is required to investigate relevant clinical aspects, eventually leading to clinical studies.

4. Conclusion

This study evaluated the biosynthesis of AgNPs using OFE and their antitumor activities against MCF7 and T47D cancer cells. The AgNPs

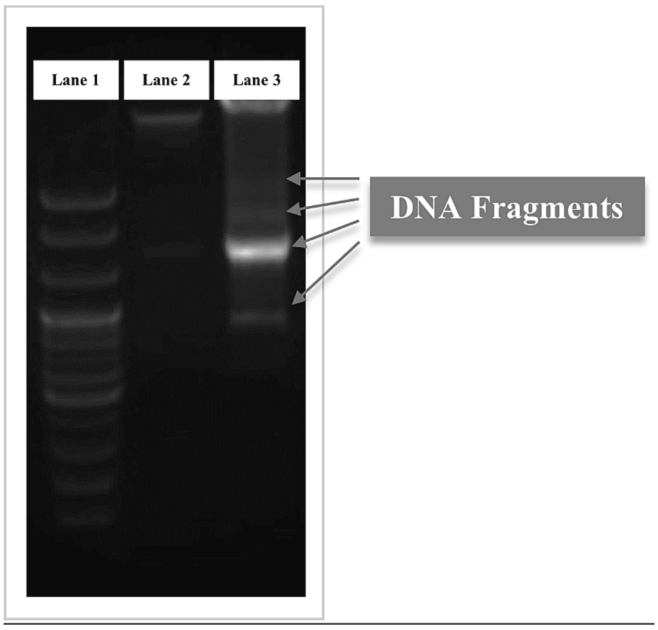

Fig. 10. DNA fragmentation of treated T47D cells; (Lane 1) DNA marker (BioFACT TM 100 bp DNA Ladder), (Lane 2) untreated cells (control), and (Lane 3) treated cells with 200 µg/mL AgNP-OFE. Gray arrows designate the fragmented DNA of treated cells.

exhibited significant anticancer activity against both MCF7 and T47D cells, and the AgNP were more effective than OFE at inhibiting the proliferation of MCF7 and T47D. The cytotoxic activity of AgNPs-OFE was high in the T47D cancer cells, with an IC_{50} of 77 µg/mL. Relevant techniques and other analyses were used for characterization and anticancer properties, and DNA fragmentation and cancer cell apoptosis were observed. This study contributes considerably to the literature because it demonstrated the feasibility of using OFE in green synthesizing AgNPs, which were stable and had an acceptable particle size and shape, as well as other desirable characteristics, including anticancer properties against the selected *in vitro* cancer cells. The results imply the potential therapeutic value of the green synthesized AgNPs and their potential for further development as anticancer drugs; however, further investigation is required. Concerns about their toxic effects on humans and the natural environment remain. Therefore, future studies on *in vivo* experiments are needed, along with more inquiries regarding their safety and toxicity before their application in biomedicine.

Declaration of Competing Interest

The authors declare that they have no known competing financial interests or personal relationships that could have appeared to influence the work reported in this paper.

Acknowledgments

This research work was funded by Institutional Fund Projects under grant no. (IFPIP: 242-247-1443). The authors gratefully acknowledge the technical and financial support provided by the Ministry of Education and King Abdulaziz University, DSR, Jeddah, Saudi Arabia.

Author contributions

Afnan I. Felimban contributed to performing the literature search, experiments, and data analysis, preparing, and writing the manuscript. Njud S. Alharbi had the idea for the article, and contributed to supervising, critically editing, revising the manuscript, and approving its final version.

Appendix A. Supplementary material

Supplementary data to this article can be found online at https://doi.org/10.1016/j.jksus.2023.102972.

References

Afreen, A., Ahmed, R., Mehboob, S., et al., 2020. Phytochemical-assisted biosynthesis of silver nanoparticles from *Ajuga bracteosa* for biomedical applications. Mater. Res. Express 7, 075404. https://doi.org/10.1088/2053-1591/aba5d0.

Amooaghaie, R., Saeri, M.R., Azizi, M., 2015. Synthesis, characterization and biocompatibility of silver nanoparticles synthesized from *Nigella sativa* leaf extract in comparison with chemical silver nanoparticles. Ecotoxicol. Environ. Saf. 120, 400–408. https://doi.org/10.1016/j.ecoenv.2015.06.025.

Asimuddin, M., Shaik, M.R., Adil, S.F., et al., 2020. *Azadirachta indica* based biosynthesis of silver nanoparticles and evaluation of their antibacterial and cytotoxic effects. J. King Saud Univ. Sci. 32, 648–656. https://doi.org/10.1016/j.jksus.2018.09.014.

Bhat, M.P., Kumar, R.S., Rudrappa, M., et al., 2022. Bio-inspired silver nanoparticles from *Artocarpus lakoocha* fruit extract and evaluation of their antibacterial activity and anticancer activity on human prostate cancer cell line. Appl. Nanosci. 1–11. https://doi.org/10.1007/s13204-022-02381-1.

Farahani, A.F., Hamdi, S.M.M., Mirzaee, A., 2022. GC/MS analysis and phyto-synthesis of silver nanoparticles using amygdalus spinosissima extract: Antibacterial, antioxidant effects, anticancer and apoptotic effects. Avicenna J. Med. Biotechnol. 14, 223–232. https://doi.org/10.18502/ajmb.v14i3.9829.

Foldbjerg, R., Olesen, P., Hougaard, M., et al., 2009. PVP-coated silver nanoparticles and silver ions induce reactive oxygen species, apoptosis and necrosis in THP-1 monocytes. Toxicol. Lett. 190, 156–162. https://doi.org/10.1016/j.toxlet.2009.07.009.

Grande, R., Sisto, F., Puca, V., et al., 2020. Antimicrobial and antibiofilm activities of new synthesized silver ultra-nanoclusters (SUNCs) against Helicobacter pylori. Front. Microbiol. 11, 1705. https://doi.org/10.3389/fmicb.2020.01705.

Hashemi, S.F., Tasharrofi, N., Saber, M.M., 2020. Green synthesis of silver nanoparticles using *Teucrium polium* leaf extract and assessment of their antitumor effects against MNK45 human gastric cancer cell line. J. Mol. Struct. 1208, 127889 https://doi.org/10.1016/j.molstruc.2020.127889.

Herceg, Z., Hainaut, P., 2007. Genetic and epigenetic alterations as biomarkers for cancer detection, diagnosis and prognosis. Mol. Oncol. 1, 26–41. https://doi.org/10.1016/j.molonc.2007.01.004.

Jang, S.J., Yang, I.J., Tettey, C.O., Kim, K.M., Shin, H.M., 2016. In-vitro anticancer activity of green synthesized silver nanoparticles on MCF-7 human breast cancer cells. Mater. Sci. Eng. C 68, 430–435. https://doi.org/10.1016/j.msec.2016.03.101.

Khatik, N., 2022. Green synthesis of nanomaterials and their utilization as potential vehicles for targeted cancer drug delivery. Nanomedicine 10, 114–121. https://doi.org/10.13189/app.2022.100205.

Kloverpris, H., Fomsgaard, A., Handley, A., et al., 2010. Dimethyl sulfoxide (DMSO) exposure to human peripheral blood mononuclear cells (PBMCs) abolish T cell responses only in high concentrations and following coincubation for more than two hours. J. Immunol. Methods 356, 70–78. https://doi.org/10.1016/j.jim.2010.01.014.

Kredy, H.M., 2018. The effect of pH, temperature on the green synthesis and biochemical activities of silver nanoparticles from *Lawsonia inermis* extract. J. Pharm. Sci. Res. 10, 2022–2026. https://www.jpsr.pharmainfo.in/Documents/Volumes/vol10Issue08/jpsr10081835.pdf.

Lee, K.X., Shameli, K., Mohamad, S.E., Yew, Y.P., Mohamed Isa, E.D., et al., 2019. Bio-mediated synthesis and characterisation of silver nanocarrier, and its potent anticancer action. Nanomaterials 9, 1423. https://doi.org/10.3390/nano9101423.

Li, G., He, D., Qian, Y., et al., 2012. Fungus-mediated green synthesis of silver nanoparticles using *Aspergillus terreus*. Int. J. Mol. Sci. 13, 466–476. https://doi.org/10.3390/ijms13010466.

Ma, D., Kanisha Chelliah, C.K., Alharbi, N.S., et al., 2021. *Chrysanthemum morifolium* extract mediated Ag NPs improved the cytotoxicity effect in A549 lung cancer cells. J. King Saud Univ. Sci. 33, 101269 https://doi.org/10.1016/j.jksus.2020.101269.

McDonald, S., Prenzler, P.D., Antolovich, M., Robards, K., 2001. Phenolic content and antioxidant activity of olive extracts. Food Chem. 73, 73–84. https://doi.org/10.1016/S0308-8146(00)00288-0.

Mittal, J., Pal, U., Sharma, L., et al., 2020. Unveiling the cytotoxicity of phytosynthesised silver nanoparticles using Tinospora cordifolia leaves against human lung adenocarcinoma A549 cell line. IET Nanobiotechnol. 14, 230–238. https://doi.org/10.1049/iet-nbt.2019.0335.

Mohanta, Y.K., Panda, S.K., Biswas, K., et al., 2016. Biogenic synthesis of silver nanoparticles from *Cassia fistula* (Linn.): in vitro assessment of their antioxidant, antimicrobial and cytotoxic activities. IET Nanobiotechnol. 10, 438–444. https://doi.org/10.1049/iet-nbt.2015.0104.

Nguyen, V.T., 2020. Sunlight-driven synthesis of silver nanoparticles using pomelo peel extract and antibacterial testing. J. Chem. 2020, 1–9. https://doi.org/10.1155/2020/6407081.

Que, Y.M., Fan, X.Q., Lin, X.J., Jiang, X.L., Hu, P.P., Tong, X.Y., Tan, Q.Y., 2019. Size dependent anti-invasiveness of silver nanoparticles in lung cancer cells. RSC Adv. 9, 21134–21138. https://doi.org/10.1039/C9RA03662H.

Rajendran, R., Pullani, S., Thavamurugan, S., Radhika, R., Lakshmi Prabha, A., 2022. Green fabrication of silver nanoparticles from *Salvia* species extracts: characterization and anticancer activities against A549 human lung cancer cell line. Appl. Nanosci. 1–14. https://doi.org/10.1007/s13204-021-02130-w.

Rajivgandhi, G.N., Ramachandran, G., Kannan, M.R., et al., 2022. Photocatalytic degradation and anti-cancer activity of biologically synthesized Ag NPs for inhibit the MCF-7 breast cancer cells. J. King Saud Univ. Sci. 34, 101725 https://doi.org/10.1016/j.jksus.2021.101725.

Raut, R.W., Mendhulkar, V.D., Kashid, S.B., 2014. Photosensitized synthesis of silver nanoparticles using Withania somnifera leaf powder and silver nitrate. J. Photochem. Photobiol. B 5 (132), 45–55. https://doi.org/10.1016/j.jphotobiol.2014.02.001.

Rawat, V., Sharma, A., Bhatt, V.P., Singh, R.P., Maurya, I.K., 2020. Sunlight mediated green synthesis of silver nanoparticles using Polygonatum graminifolium leaf extract and their antibacterial activity. Mater. Today:. Proc. 29, 911–916. https://doi.org/10.1016/j.matpr.2020.05.274.

Salem, S.S., Fouda, A., 2021. Green synthesis of metallic nanoparticles and their prospective biotechnological applications: an overview. Biol. Trace Elem. Res. 199, 344–370. https://doi.org/10.1007/s12011-020-02138-3.

Saravanan, C., Rajesh, R., Kaviarasan, T., et al., 2017. Synthesis of silver nanoparticles using bacterial exopolysaccharide and its application for degradation of azo-dyes. Biotechnol. Rep. (Amst.) 15, 33–40. https://doi.org/10.1016/j.btre.2017.02.006.

Saware, K., Venkataraman, A., 2014. Biosynthesis and characterization of stable silver nanoparticles using Ficus religiosa leaf extract: A mechanism perspective. J. Clust. Sci. 25, 1157–1171. https://doi.org/10.1007/s10876-014-0697-1.

Selvan, D.A., Mahendiran, D., Kumar, R.S., Rahiman, A.K., 2018. Garlic, green tea and turmeric extracts-mediated green synthesis of silver nanoparticles: Phytochemical, antioxidant and in vitro cytotoxicity studies. J. Photochem. Photobiol. B Biol. 180, 243–252. https://doi.org/10.1016/j.jphotobiol.2018.02.014.

Shukla, R., Nune, S.K., Chanda, N., et al., 2008. Soybeans as a phytochemical reservoir for the production and stabilization of biocompatible gold nanoparticles. Small 4, 1425–1436. https://doi.org/10.1002/smll.200800525.

Singh, S.P., Mishra, A., Shyanti, R.K., Singh, R.P., Acharya, A., 2021. Silver nanoparticles synthesized using Carica papaya leaf extract (AgNPs-PLE) causes cell cycle arrest and apoptosis in human prostate (DU145) cancer cells. Biol. Trace Elem. Res. 199, 1316–1331. https://doi.org/10.1007/s12011-020-02255-z.

Some, S., Bulut, O., Biswas, K., et al., 2019. Effect of feed supplementation with biosynthesized silver nanoparticles using leaf extract of Morus indica L. V1 on Bombyx mori L. (Lepidoptera: Bombycidae). Sci. Rep. 9, 1–13. https://doi.org/10.1038/s41598-019-50906-6.

Sung, H., Ferlay, J., Siegel, R.L., et al., 2021. Global cancer statistics 2020: GLOBOCAN estimates of incidence and mortality worldwide for 36 cancers in 185 countries.CA Cancer. J. Clin. 71, 209–249. https://doi.org/10.1016/j.acra.2021.04.019.